NASA Technical Memorandum 100052

Development of Subminiature Multi-Sensor Hot-Wire Probes

Russell V. Westphal, Phillip M. Ligrani, and Fred R. Lemos

March 1988

National Aeronautics and Space Administration

NASA Technical Memorandum 100052

Development of Subminiature Multi-Sensor Hot-Wire Probes

Russell V. Westphal, Ames Research Center, Moffett Field, California
Phillip M. Ligrani, Naval Postgraduate School, Monterey, California
Fred R. Lemos, Ames Research Center, Moffett Field, California

March 1988

National Aeronautics and
Space Administration

Ames Research Center
Moffett Field, California 94035

SYMBOLS

C_f	skin friction coefficient, $C_f = \tau_w/(1/2\rho U_e^2)$
d	hot-wire sensor diameter
E	hot-wire anemometer output voltage
E_0	constant in hot-wire cooling equation
$E_{uu}(n)$, $E_{vv}(n)$	relative spectral energy per unit frequency for u or v components
$f(E,\delta)$	function used for angular calibration, see equation 1
L	typical length
l	hot-wire sensing length
m	exponent in hot-wire cooling equation
n	frequency
Re_L	typical Reynolds number, $Re_L = UL/\nu$
Re_θ	momentum thickness Reynolds number, $Re_\theta = U_e\theta/\nu$
r	ratio of hot-wire sensor operating resistance to cold resistance
s	crossed hot-wire sensor separation
U_τ	friction velocity, $U_\tau = \sqrt{\tau_w/\rho}$
u, v, w	instantaneous fluctuating velocity components in X, Y, Z directions
U, V, W	mean velocities in X, Y, Z directions
X, Y, Z	right-hand Cartesian streamwise, gradient, and spanwise directions
δ	nominal angle of rotation used for hot-wire angular calibration
δ^*	boundary layer displacement thickness, $\delta^* = \int_0^\infty (1 - U/U_e)dY$
δ_{99}	boundary layer thickness, defined as $Y(U/U_e = 0.99)$
θ	boundary layer momentum thickness, $\theta = \int_0^\infty U/U_e(1 - U/U_e)dY$
ν	air kinematic viscosity
ρ	air density
τ_w	streamwise mean skin friction
ψ	"effective" hot-wire angle, from calibration
$()_e$	refers to local free stream conditions
$()^+$	length or velocity made dimensionless by ν and U_τ

DEVELOPMENT OF SUBMINIATURE MULTI-SENSOR HOT-WIRE PROBES

Russell V. Westphal, Phillip M. Ligrani,[1] and Fred R. Lemos

Ames Research Center

1. SUMMARY

Limitations on the spatial resolution of hot-wire probes have precluded accurate measurements of Reynolds stresses very near ($Y+ < 100$) solid surfaces in practical aerodynamic flows, and motivated the present effort to develop substantially smaller sensors. These sensors are to be used in single, X-array, and three-wire probes for measurements requiring better spatial resolution than obtained with the smallest conventional probes, whose length and diameter are typically 400-1000 μm and 2-5 μm, respectively. The sensors developed in the present study have a diameter of 0.63 μm and length of $\sim$ 200 μm.

A new sensor fabrication procedure was developed using an acid jet to etch the Wollaston wire without any additional replating to control the sensing length. The new procedure allowed multi-sensor probes to be constructed with good control of wire orientations. The subminiature probes were operated using commercial hot-wire circuitry, but some changes in the electronics and procedures were needed to reduce probe breakage and optimize frequency response. Identical calibration methods to those employed for conventional probes were found satisfactory for the subminiature probes. The major disadvantage of the new probes is that manfacture is more complex than for conventional-sized probes, requiring special equipment. Careful handling is required both during manufacture and operation. Also, drift was occasionally observed to be about twice that from conventional probes, resulting in slightly larger measurement uncertainties.

The subminiature probes were tested using measurements in a constant-pressure turbulent boundary layer. Measurements of mean statistical quantities, including Reynolds stresses, and spectra were obtained to evaluate the performance of the subminiature sensors compared with results from conventional probes. The results indicate that the new probes can give improved measurements of turbulence quantities near a surface in spite of the difficulties cited above, and that the anisotropic nature of the flow has a strong influence on the relative errors in different quantities caused by spatial resolution effects. Therefore, classical theories based on the assumption of isotropic turbulence cannot be expected to provide an accurate estimate of spatial resolution effects for X-wires near a wall.

[1]Naval Postgraduate School, Monterey, CA.

2. INTRODUCTION

For typical aerodynamic wall-bounded turbulent flows, a high degree of spatial resolution is required near the surface because of the wide range of turbulence length scales present. The relevant inner length scale for flat-plate boundary layers is the viscous length ν/U_τ. One inner unit typically corresponds to a physcial length of 15-100 μm in low-speed aerodynamic flows. Although a fluid of higher viscosity can be used to enlarge the physical dimension of the viscous length, this approach will always lead to a need for specialized facilities which must also be extremely large to maintain the desired Reynolds number ($Re = U_\tau L/\nu$, where L denotes a typical length scale). Another approach, reduction of the shear velocity U_τ, requires extremely low flow velocities, particularly if air is employed as the working fluid, and will again lead to large facilities. To avoid the problems associated with specialized facilities or low velocities, the present study is focused on development and testing of subminiature-sized sensors.

Willmarth and Bogar (1977) made one of the earliest attempts to develop and use ultra-small hot-wire probes for turbulence measurements. Their miniature crossed-wire probe had a wire length and spacing of about 100 μm, and used a sensor diameter of 0.6 μm. Because the orientation of each wire could not be well controlled, unique calibration procedures were required, along with tables of calibration data to process the instantaneous pair of signals from the two sensors. During their experiments, signals were recorded outside the range of the calibration grid, which, according to the authors, indicated small scale activity with length scales less than 2.5 times the viscous length. Willmarth and Sharma (1984) later developed pairs of horizontally mounted hot-wires, each having a length of 25 μm, and spaced about 200 μm apart. These sensors were operated in constant-current mode to minimize electronic noise. The authors also indicated other difficulties: significant drift, frequent breakage, and length-to-diameter ratios of about 50 resulting in very low sensitivity and reduced frequency response caused by heat loss through the sensor supports (Lord 1981, Perry 1982, Kuhn and Dressler 1985).

The manufacturing techniques of Willmarth and Sharma (1984) formed the basis of methods later used by Ligrani and Bradshaw (1987a) to fabricate single-element horizontal hot-wire probes. Sensor elements were made starting with a silver-coated length of Platinum-Rhodium wire (manufactured by the Wollaston process), whose (uncoated) diameter was 0.6 μm. A multi-step procedure was then employed for shaping, etching, re-plating, and cleaning each element. Sensors were operated in constant temperature mode, without most of the difficulties encountered by Willmarth and Sharma. With these subminiature sensors, Ligrani and Bradshaw (1987b) then measured new characteristics in the viscous sublayer, showing that sensor length must be less than 20-25 viscous lengths to avoid significant spatial resolution difficulties with a horizontal wire. Though adequate alignment for single-sensor probes may be obtained with the fabrication method used in these studies, the procedures would be difficult to apply to multi-sensor probes, which require accurate control of the relative orientation of several sensing elements.

Nakayama and Westphal (1986) present experimental results showing some of the errors caused by finite spatial resolution of an X-wire probe in a boundary layer. Sensor lengths varied between 0.8 and 2.6 mm, with diameters ranging from 2.5 to 5.0 μm. Longer crossed-wire lengths resulted in reduced Reynolds stress magnitudes, whereas larger wire spacing resulted in larger measured cross-stream stresses. Overall, increased length and spacing tended to make the turbulence appear to be more isotropic.

A review of previous work addressing problems of spatial resolution with hot-wires is given by Nakayama and Westphal (1986) and Ligrani and Bradshaw (1987b). Among those who have considered spatial resolution effects resulting from crossed-wire and other multiple-wire probes are Wyngaard (1968, 1969), Bremhorst (1972), and Roberts (1973), who give correction schemes which are valid only when small-scale turbulence is locally *isotropic*, or the local three-dimensional (3-D) turbulence spectrum is known. The present study and that of Nakayama and Westphal (1986) address spatial resolution of multi-wire probes for measurements in turbulent boundary layers, where even small-scale motions are strongly *anisotropic*, and no detailed representation for the 3-D turbulence spectrum exists.

Using the procedure given by Ligrani (1984) as a starting point, improved means have been developed to fabricate subminiature hot-wire probes. The methods developed here are advantageous compared to previous techniques because they allow accurate control of sensing element orientation such that good multi-sensor probes can be produced. Both single horizontal-wire and two-element X-wire probe configurations are described, along with detailed manufacturing instructions. Probe operation and performance characteristics are then given, including all modifications required to operate subminiature sensors differently than standard-sized probes. Measurements within a flat-plate turbulent boundary layer were made to show the capabilities of subminiature hot-wire probes for obtaining turbulence measurements. Finally, a few concluding remarks give the authors' evaluation of the prospects for using subminiature probes in future work.

The helpful suggestions of Mr. K. R. Raman are gratefully acknowledged. Mr. Charles Hooper has written and helped test much of the software used for the experiments. Funds for the support of one author (P.M.L.) were provided by Ames Research Center, through NASA-Navy Interagency Agreement number A41462C.

3. SENSOR FABRICATION

3.1 Sensor Description

The sensors themselves were 90% platinum/ 10% rhodium wire, having a diameter of 0.625 μm, according to the manufacturer (see table 1). As indicated in the detailed con-

struction procedure which follows (see section 3.2), the Wollaston wire with silver coating ($d = 35$ μm) was initially mounted between two prongs and a portion of the silver was etched away, leaving a small segment of exposed platinum/rhodium wire. Thus, the exposed sensing element was supported between two larger-diameter segments of silver, which are epoxied to two nickel support prongs. Here, nickel was used rather than stainless steel because it is more easily machined. This mounting is different from the one employed by Willmarth and Sharma (1984), or Ligrani and Bradshaw (1987a), who bent a Wollaston wire segment into a loop, soldered the loop to support needles, then etched a small portion of silver away at the tip. The ends of the etched wire were then plated with small amounts of copper to achieve the desired active length. With the present procedures, nominal platinum/rhodium wire sensing lengths were 160-220 μm, providing length-to-diameter ratios of about 250-350.

3.1.1 Horizontal wire sensors. Figure 1 shows the configuration of the horizontal wire sensors. The two nickel prongs were 1.1 to 1.3 mm apart at the ends where the Wollaston wire was attached. These prongs were about 9.5 mm long, and tapered over 6.4 mm from 0.38 mm nominal diameter to 0.06 diameter at the tip. The prongs were pointed outwards from a 1.58 mm diameter ceramic cylinder wherein they were mounted 0.64 mm apart. A small amount of nonconductive epoxy was placed between these prongs to minimize the possibility of vibration at the prong tips. The ceramic cylinder was used to provide insulation for electrical connections, and was contained in a steel tube, 75 mm long with inner and outer diameters of 1.6 and 3.2 mm, respectively. The tube was designed so that it could be rotated and oriented accurately within a cylinder connected directly to the traversing mechanism. Orientation was set by means of two pins on opposite sides of the tube which fit into slots located at different circumferential positions on the mounting cylinder.

3.1.2 Crossed wire sensors. Each individual sensor in a crossed configuration was the same as for the horizontal wire, except for orientation. The crossed-wire probe configuration is shown in figure 2. Here, the nickel prong tips were staggered so that sensors could be oriented at an angle close to 45° with respect to the probe axis. The actual angles of the sensors were usually within 1 to 2° of the desired value, as determined from calibration. The sensor separation was 200-400 μm. The crossed-wire probe required special tilting during the etching and cleaning process (see section 3.2) so that silver could be removed from each sensor individually.

3.2 Fabrication Procedure

Several special equipment items were needed to construct subminiature hot-wire sensors: (1) a microscope with a zoom magnification adjustment between 50x and 210x, (2) a micromanipulator capable of translation along three axes and rotation about two axes, (3) a light source to provide illumination for microscope viewing, (4) a controller to regulate the

amount of current during etching, and (5) flasks to contain etching and washing solutions connected to a pipette used to direct the etching and washing jets. Equipment items are listed in table 1 along with their manufacturer. The light source, microscope, micromanipulator, and flasks were mounted on a granite table to reduce vibrations of the work during fabrication. Additional information on the equipment employed is given in table 1.

The microscope and light source are shown in figure 3. The microscope is binocular, capable of magnification up to 210 power, and has a camera mount to allow photographs to be taken. The entire system was mounted on a stand allowing translation in two directions and rotation about one axis. The light source had an adjustable lamp with intensity settings, and two flexible fiber-optic tentacles used to direct the lighting. A variety of filters could be employed with the light system; a clear glass filter was used for the present work. The micromanipulator used to control the sensor tip position and orientation during manufacture is shown in figure 4. A device allowing rotation about two axes was mounted on a miniature mill table capable of translation in two directions. This was then fixed to a small microscope stand used to adjust vertical position. The etching current controller and flask system are described later in this section.

The manufacturing procedure details are now given in four parts: (1) mounting the (unetched) wire, (2) sensor etching, (3) sensor washing, and (4) sensor length check. Photographs showing the sensor at various steps in the manufacturing process are shown in figures 5a-c.

3.2.1 Mounting the (unetched) wire. Before attempts were made to mount the Wollaston wire, several cut lengths were first produced, each with a length as close as possible to the distance between the outsides of the two support prongs, generally 1.1-1.3 mm. Both wire and scale were viewed using the microscope while cutting the wire with an exacto knife.

In order to attach the Wollaston wire to the two support prongs, an electrically conductive epoxy, which is tolerant of the etching acid, was employed. A miniature broaching tool, having a pointed tip with a 0.13 mm square cross-section (ordinarly used in watch repair), was used to place epoxy on the prongs used to support the Wollaston wire. A small amount of epoxy, about half a millimeter in diameter, was placed as a "crown" on the end of each prong tip.

To place the Wollaston wire on the support prongs, a very small spot of epoxy was placed on the tip of the broaching tool, then the cut Wollaston wire segment was picked up by one end. The part of the wire segment hanging farthest from the broaching tool was then located on the tip of one prong. The other wire end (connected to the broaching tool) was then placed on the other prong tip. The wire was then carefully aligned and centered with respect to the prongs, and pushed further into the epoxy using the broaching tool. Each end of the Wollaston wire was oriented to be as near the center of each prong tip as possible. The first application of epoxy was cured, then small additional amounts of epoxy were added to further coat the Wollaston wire connections at the end of each support prong. Final sensor

orientation depends upon the mounting of the unetched wire and the positions of the prong tips, and is determined from calibration as described in section 4.3 and the Appendix.

The epoxy will cure at room temperature in 3 to 4 hr; this was accelerated to about 2 hr using an oven to provide a temperature of around $40C$. Higher temperatures are not recommended since they may result in thermal stresses added to the Wollaston wire. Figure 5a shows a photograph of the probe tip at the completion of the epoxying procedure.

Wires for the crossed-wire probe were mounted in the same way as for the horizontal wire probe.

Solder was also tried as a means to attach the Wollaston wire to support prongs, but sensors attached in this way broke frequently during etching. This was believed to be due to heat from the soldering iron which may have imparted thermal stresses to the silver and the platinum/rhodium, which have different thermal expansion coefficients. A low-temperature solder might work as well as the epoxy, but was not tried when epoxy proved successful.

3.2.2 Sensor etching. Etching was required to remove the silver plating from the Wollaston wire so that a segment of platinum/rhodium wire was completely exposed. The equipment used during the etching procedure included a current controller, etching and washing flasks and piping, microscope, light source, and micromanipulators. Figure 5b is a photograph showing the sensor during etching.

The flask and piping system used for etching (fig. 6) consisted of a glass reservoir containing 5% Nitric acid connected by a valve to a tube connected to a pipette (0.1 mm inner diameter). With the valve open, a small laminar jet of etching fluid exited the pipette and was directed onto the sensor. The pipette was mounted on a micromanipulator for fine position adjustment in two directions in the horizontal plane, and coarse adjustment in the vertical direction (see fig. 6).

In order to provide current for etching, a platinum wire was inserted in the reservoir of Nitric acid, and connected to the negative output terminal (cathode) of the etching current controller. The positive terminal (anode) was connected to the probe prongs, so that with the probe tip in the acid flow, the electric circuit was closed. Manufacturing details for the etching current controller are available from the authors. It has coarse and fine current adjustment knobs, a current level indicator, and a selection knob for the following current ranges: 10-100 μA, 100-1000 μA, 1-10 mA, and 10-100 mA. At 150 μA, the device should produce about 1.5 volts. The device is essentially a DC voltage source, maintaining constant DC potential across its output terminals so that current decreases as resistance increases. This is advantageous during the etching procedure since the resistance of the probe tip increases as etching proceeds and silver plating is removed, which, ideally, would result in constant current density at the probe tip.

For present probe configurations, manufactured using an acid jet from a 0.1 mm inner diameter pipette, the lowest current range was used initially without adjusting the current level. During the first part of etching process, the current was approximately constant at 15 μA. The acid jet was moved perpendicular to the sensor, back and forth, with no motion along the length of the sensor, resulting in a slight taper of the silver plating adjacent to the sensor. As this process proceeded, the current level dropped slowly until, when the silver was completely removed, the current was less than 1 μA. Approximately 10 min are required to competely remove all of the silver over a 200 μm length.

Occasionally it appeared that some small silver particles remained after the usual etching procedure. When this occured, etching was resumed for a few minutes with the current controller set to its $1 - 10$ mA range, and adjusted so that about .04 mA passed through the circuit. Also, it should be noted that small amounts of oxide sometimes appeared on the silver which affected the uniformity of silver removal and slowed the etching process.

In the first attempts at etching, ordinary tap water was used as the solvent for the 5% Nitric acid. As a result, small crystalline deposits formed on the probe tip, and silver etching occured nonuniformly. To avoid these difficulties, clean distilled water which was passed through a quartz filter before being used in solution was required. Some experimentation was done with using a surfactant in an attempt to reduce surface tension and thus also reduce the forces on the probe tip during etching. However, it did not appear that these forces were responsible for difficulties with breakage during etching: these problems were eventually attributed to soldering the Wollaston wire to the supports, as previously described.

At the completion of the etching process the appearance of the probe tip was as shown in figure 5c, in which the exposed area ends abrubtly, and the adjacent (plated) wire is hardly tapered from its unetched diameter of 35 μm. The small separated wakes from the tips of the silver plating will cover small portions of the ends of the sensing wire, which are believed to approximately correspond with regions where the mean wire temperature varies with sensor length during operation. For a 200 μm sensor, these regions cover about 10% of each end of the sensor, and are referred to as the "cold length" (Perry 1982). It is believed that the effects of the abrupt transition are confined to the cold regions, and should not significantly influence the sensor response.

Etching each (slanted) sensor in the crossed-wire array was similar to horizontal wire etching, except the micromanipulator required a compound angle tilting mechanism so that each sensor could be etched individually. Extra care was required when etching the second wire so that the etch jet and particles of silver would not break the previously etched sensor. Crossed-wire sensors with separations as small as 0.2 mm have been etched in this way. Figure 7 shows a completed subminiature crossed-wire probe and a photograph of the same probe prior to etching.

3.2.3 Sensor washing. The sensors were washed after etching to remove any residual acid solution, following previous observations (Ligrani 1984, Ligrani and Bradshaw 1987a) that significant drift is observed if sensors are not washed in this way. Distilled water was passed through a quartz filter before being used for washing. Using a reservoir and pipette identical to that employed during etching, the stream of distilled water was translated back and forth along the length of the sensor several times to thoroughly remove any acid residue. The procedure required about 3 min.

3.2.4 Sensor length check. After construction, sensor length was measured optically using a calibrated scale within the microscope. The measured length should be about the same as that determined from the length computed from measurment of the probe resistance and using the nominal resistivity of 0.625 μm diameter platinum/10% rhodium wire (0.58 ohms/μm). Otherwise, one of a number of problems are indicated, including silver bits on a partially etched sensor or bad electrical connections at the wire/support joint (Ligrani 1984).

4. PROBE OPERATION AND PERFORMANCE

The subminiature sensors were operated at 20 to 80% overheat resistances (resistance ratios of 1.2 to 1.8), similar to conventional sensors. However, the subminiature sensors possess much larger resistance than conventional sensors. Therefore, operation of the probes with commercial bridges is somewhat different than when conventional probes are used; details are given below.

The subminiature crossed-wire probes used were fragile; even a slight jarring of the probes was found to cause breakage of the sensors. Thus, special care was required when handling probes; additionally, the traversing mechanism was designed so that the probes could be installed as the last step prior to making measurements. This minimized the handling of the probes and the chance of mechanical breakage.

Subminiature hot-wire sensors seemed to be more likely to burn-out when operated at resistance ratios greater than 1.6. After a short operating time, a 10 to 15 ohm (about 10%) change in cold resistance sometimes occured, followed by burn-out. Inspection using the microscope revealed discoloration near the center of the sensor, with a small gap in the middle where the sensing wire was severed. This experience led us to select 1.35 as the operating resistance ratio for most of the measurements with subminiature probes. Sensors operated at this value were never observed to burn-out; all failures were attributed to mechanical breakage. It was speculated that the mechanical breakage was caused either by impact of dirt particles or by vibration of the wire supports. Most subminiature sensors survived less than 10 hr of operation – far less than the (indefinite) lifetimes experienced with conventional 5 μm tungsten sensors.

The voltages from the subminiature sensors used in this study occasionally drifted. Several tests were performed with constant flow velocity at a resistance ratios of 1.35; usually, less than 1 % change in mean voltage was observed over several hours' operation. However, changes of a few percent were sometimes noted over less than 15 min. The drift did not appear to correlate with sensor age, and it is not believed that re-washing would be useful since all sensors were very thoroughly washed. Such behavior would add to the uncertainty in mean measurements, but would have less effect on the measured turbulence stresses.

4.1 Constant-Temperature Bridge Operation and Adjustment

To operate the subminiature hot-wire sensors, 55M series anemometer bridge electronics manufactured by DISA (now DANTEC) were employed. Each 55M system included a main unit (55M01), standard bridge (55M10), and power pack (55M05) (see the DISA Instruction Manual). The hot-wire bridge electronics were modified to accomodate the higher sensor resistance (greater than 100 ohms) by adding 2 and 4 kohm metal-foil precision resistors to the decade resistance controller. With the 20 to 1 bridge of the DISA 55M10, these correspond to sensor resistances of 100 and 200 ohms, respectively. Metal foil (rather than wire-wound or carbon) resistors were employed because of their low inductance and small temperature coefficient (Perry 1982). A 200 μm long sensor operated at a resistance ratio of 1.8 then required a 209 ohm hot resistance setting. When using such resistance values, better response to square wave tests was obtained when one 200 ohm element (rather than two 100 ohm resistors in series) were added to the bridge circuit, probably because of inherent impedance contained in each resistance element.

The bridge of the 55M system contains a provision to set amplifier response chararcteristics either to FLAT or SHAPED frequency response modes by setting a small switch within the bridge module. In FLAT mode, the operating point of the amplifier is adjusted by means of a potentiometer accessible through the front panel. In the SHAPED mode, the amplifier gain, which has a very high value at DC, declines at higher frequency so that the gain at 100 kHz then equals the gain at all frequencies in the FLAT mode of operation (ref. DISA Instruction Manual). Adjustment of the amplifier operating point provided an important means to change the response characteristics of the subminiature hot-wire probes when subject to square-wave testing. Without this adjustment, bridge oscillation could sometimes lead to sensor breakage; this may explain the difficulties encountered by Miller et al. (1987) in operating small sensors with the DISA bridge.

4.2 Square-Wave Response

Square-wave tests were used to adjust the circuitry of hot-wire bridges so that sensors could be operated with optimal frequency response. Ordinarily, five different adjustments

may be made on the DISA electronics to optimize the response of a hot-wire probe to a square-wave test: (1) amplifier operating point (offset voltage, FLAT mode only), (2) feedback amplifier gain (GAIN), (3) feedback amplifier high-frequency filter (HF FILTER), and (4,5) two adjustments to compensate for cable impedance within the bridge circuit (ordinarily labelled Q and L). When the GAIN and HF FILTER settings were changed, the bridge was set into a stand-by mode of operation. Without this precaution, it was believed that one subminiature probe was destroyed in early testing, perhaps because noise was generated during a switch position change.

Changing cable impedance adjustments (Q and L) resulted in almost no change in sensor response characteristics, probably because DISA bridges operate away from normal operating points with subminiature sensors. Improved response was obtained by reducing the length of the cable between the bridge and sensor from 5 to 1.5 m, while continuing to employ the 5 m compensation unit. It was found that good frequency response was usually obtained with both GAIN and HF FILTER set to 1, then adjusting only the offset voltage to optimize the square-wave response.

Figures 8a-c show oscilloscope traces of the bridge output response to square-wave tests, obtained using a probe having 130 ohms cold resistance and connected to the bridge with a 1.5 m long cable. The first of the photographs (fig. 8a) is for a resistance ratio of 1.2, with a GAIN setting of 3 and HF FILTER setting of 1. Some high-order oscillations are evident which result in an overall response time of about 25 μsec. Improved performance with a response time of approximately 12 μsec and without high-order oscillations is evident in figure 8b. For this case, the resistance ratio was increased to 1.5, and the GAIN setting was decreased to 1. A slight further improvement in response is evident in figure 8c, where a resistance ratio of 1.65 was employed.

4.3 Probe Calibration

The subminiature probes were calibrated separately for sensitivity to varying velocity and varying flow angle; the methods used were the same as for conventional sensors. Details of this procedure along with references are provided in the Appendix.

Figure 9 shows typical calibration results of anemometer output versus velocity with probe orientation fixed for both sensors of a subminiature X-wire, over a 3:1 range of variation in velocity. The observed behavior follows the calibration function[2] $U^m = B(E^2 - E_O^2)$, with a value of m smaller than generally employed for 5 μm diameter sensors operated under similar conditions (0.37 versus 0.45). This smaller value of m at a lower wire Reynolds number is consistent with the trend of data tabulated by Blackwelder (1981). In fitting the values of B and E_0^2 once m had been selected, typical root-mean-square errors of about 0.5%

[2] At this stage, the cosine term arising from the (unspecified but constant) orientation of the wires is absorbed into the constant B.

were obtained – about twice that obtained for 5 μm diameter sensors operated under the same conditions, but still considered acceptably small.

Calibration of the probes for sensitivity to variation in flow angle was performed by rotating the probes through a known angle δ about an axis perpendicular to the plane containing the sensor wire and the probe support needles (the "yaw plane"), then using the results to determine the "effective angle", ψ (see Westphal and Mehta, 1984). The angular responses for the subminiature single-sensor horizontal wire probe and both sensors of the subminiature crossed-wire probe are shown in figure 10. Note that the slope of the best-fit straight line through these results represents the tangent of the effective wire angle ψ for the cosine angular sensitivity law:

$$f(E,\delta) \equiv \cos(\delta) - \left(\frac{E^2(\delta) - E_0^2}{E^2(\delta = 0) - E_0^2}\right)^{(1/m)} = \tan(\psi)\sin(\delta) \qquad (1)$$

The cosine law seemed to fit the calibration results about as well for the subminature probes as for the larger sensors used previously.

5. BOUNDARY LAYER MEASUREMENTS

To evaluate the performance of the subminiature probes, profile measurements of mean velocity, Reynolds stresses, and higher-order products were made in a turbulent boundary layer. At a few positions, spectral estimates were also obtained. All the measurements with the subminiature probes were made at a station $X = 285$ cm; two free stream velocities were employed, 20 and 27 m/s. Only results with $U_e = 27$ m/s will be presented here. Also, the present results do not include measurements very near the surface ($Y^+ < 300$), since the purpose here is to evaluate the subminiature probes through comparison with measurements from conventional probes. The Appendix contains a brief description of the wind tunnel apparatus and measurement procedures used. For reference, table 2 gives boundary layer properties computed from velocity profile measurements made with a total pressure probe immediately downstream ($X = 295$ cm) of the measurement station used for the subminiature probes ($X = 285$ cm).

Measurements taken with subminiature single and crossed hot-wire probes will be compared with measurements made with a conventional crossed hot-wire probe in the following presentation. Table 3 gives the actual probe dimensions, along with values made dimensionless using the boundary layer parameters for $X = 295$ cm and $U_e = 27$ m/s. The abbreviations used for each probe in the following discussion are also given in the table: XN denotes the "conventional" (5 μm) X-wire probe, S1 for the subminiature horizontal single-wire probe, and X2 for the subminiature crossed hot-wire.

Figure 11 compares the mean velocity measurements and figure 12 shows the same results plotted in inner coordinates on a logarithmic scale. Though all the results are in substantial

agreement, close inspection reveals that the results from the subminiature probes show more scatter, which is attributable to the drift behavior previously discussed.

Measurements of the normal stresses $\overline{u^2}$ and $\overline{v^2}$ are shown in figures 13 and 14. The small differences in $\overline{u^2}$ are at least partly attributable to contamination from w, which is more important with crossed-wire probes than for single horizontal probes in a boundary layer. In spite of this, the $\overline{u^2}$ measurements are not strongly influenced by probe size effects over the range of Y shown, yet the $\overline{v^2}$ results show definite differences. For isotropic turbulence, Wyngaard (1968) suggested that X-wires suffer from "crosstalk" caused by finite wire separation, and averaging of fluctuations along the wire sensor. Assuming isotropic turbulence, he showed that crosstalk, if present, causes larger errors in $\overline{u^2}$, and that the averaging errors are similar for $\overline{u^2}$ and $\overline{v^2}$ (see also Nakayama and Westphal, 1986). Thus, the observation of spatial resolution errors in $\overline{v^2}$ without much error in $\overline{u^2}$ implies that the anisotropy of the turbulent motions nearer the surface is important in determining the effects of finite probe size on the various measurements.

Figure 15 shows frequency spectra of the u and v components of velocity measured near the logarithmic region. The anisotropy is evident from the differences in the shapes of these spectra: the v spectra are flatter, so that a relatively larger proportion of the energy in the v fluctuations is present at higher frequencies. Perry et al. (1986) explain this observation in terms of Townsend's attached eddy hypothesis, which further indicates that the w spectrum is expected to behave like that of u. Therefore, the reduced size of the subminiature probe is more important for measurements of $\overline{v^2}$ than for $\overline{u^2}$ or $\overline{w^2}$.

The Reynolds shear-stress measurements of figure 16 show that the subminiature probe results extrapolated to the surface agree well with the expected level as determined from independent measurement of the skin friction. The measurements from the larger probe tend to be low in the wall region, with consistently greater scatter. As was found previously (see Nakayama and Westphal, 1986), figure 17 shows that the correlation coefficient R_{uv} is somewhat insensitive to spatial resolution effects in spite of the differences in $\overline{v^2}$ and $\overline{uv}$. Also, measurements of the higher-order products such as $\overline{u^2v}$ and $\overline{u^3}$ (not reported here) with the subminiature and conventional probes showed agreement within data scatter.

6. CONCLUDING REMARKS

Subminiature single horizontal and crossed hot-wire probes have been fabricated using an improved method which allows accurate control of sensor orientation and etched (active) sensor length. With the new procedure, the final plating step in the sensor manufacture used by previous workers is eliminated. The fabrication of three-wire probes should be feasible by using the method described here.

The subminiature probes were easily operated with slightly modified, commercial anemometer electronics. However, the probes were found to be fragile and subject to breakage if high operating resistance ratios were used. Even with the precaution of limiting the resistance ratio to about 1.35, probe lifetimes greater than a few days were rare. It was not evident whether breakages *not* attributable to burn-out were caused by particles of dirt in the airstream, by probe support vibration, or by some other unknown factor. Drift of the probe output over time occured irregularly; some tests revealed no drift while other tests showed measurable drift over a few hours' time. When it occured, the mean drift of the subminiature probes was typically twice that of conventional probes – i.e., about 1/4% per hour when related to mean velocity for the conditions of the present study. Both the drift behavior and the frequency of breakage might be improved under operation in a cleaner wind tunnel.

Calibration of the subminiature probes for varying velocity and flow angle showed that the relations used for conventional probes to relate anemometer output to velocity magnitude and direction were applicable, except that a smaller value of the cooling law exponent m was required. The fit of the cooling law data showed a larger aggregate least-square error over the same velocity range than for conventional probes, but this error (0.5%) was not considered excessive. There was no need to employ complex calibration methods or peculiar response equations for the subminiature probes.

Measurements made in a turbulent boundary layer using the subminiature probes were compared with results from conventional crossed-wire and total pressure probes. The subminiature probe data generally agreed with the other methods when probe volume dimensions were unimportant. Nearer the wall, where dominant turbulence length-scales were similar to the sensor lengths, the subminiature probe gave more credible measurements of several turbulence quantities. In particular, turbulence quantities involving normal (v) component fluctuations, such as $\overline{v^2}$ and $\overline{uv}$, were higher near the wall when measured with the subminiature probe, as would be expected from finite spatial resolution effects. The near-wall measurements of $\overline{uv}$ from the subminiature probe compared well with the measured skin friction, whereas the 5 μm crossed-wire results appeared to be too low near the wall.

The new subminiature probes have been qualified for future measurements requiring improved spatial resolution. Further tests, including measurements near the surface, use in thin boundary layers with pressure gradients, and development of a three-wire probe, are planned using the results of the present study.

APPENDIX: EXPERIMENTAL DETAILS

Wind Tunnel

The measurements were performed in the Boundary Layer Wind Tunnel located in the Fluid Mechanics Laboratory (building N260) at Ames Research Center. The airfoil-bladed centrifugal blower-driven wind tunnel was fitted with an inlet dust filter, and had flow conditioning elements (a honeycomb with screens) within the settling chamber upstream of the 7.5:1 contraction preceeding the test section.

At the free stream speeds used for the present work, 20 m/s and 27 m/s, the static pressure in the test section was maintained constant as measured by sidewall pressure tappings to about 0.5% of the free stream dynamic pressure by adjustment of the height of the control wall opposite the test surface. Details of the free stream flow quality have been documented elsewhere (see Wood and Westphal, 1987); the measured r.m.s fluctuation of the u component was about 0.2% at the end of the test section over the range $U_e = 20 - 30$ m/s.

The tunnel design produces a laminar boundary layer on the contraction walls entering the 20 by 80 by 300 cm test section. A small wire (0.4 mm diameter) trip was positioned 20 cm from the contraction exit, resulting in a tripped, fully turbulent boundary layer at downstream locations. The boundary layer momentum thickness Reynolds number at the end of the test section ($X = 295$ cm) was 5950 for 20 m/s, and 8300 for 27 m/s.

Hot-Wire Measurement Procedures

The hot-wire response equations and calibration methods used were the same as described by Westphal and Mehta (1984): a variable-exponent cooling law and cosine angular sensitivity were employed. Calibrations were performed in two parts: (1) at fixed angle and varying velocity, and (2) at fixed velocity with varying yaw angle to determine the effective wire angles. The magnitude of the "pitch-up correction" (see Westphal and Mehta, 1984) was obtained by orienting the probe so that the measurement plane was at a right angle to the plane of rotation for the angular calibration. The calibrations were performed *in situ*, that is, with the probes in the free stream of the same wind tunnel as used for the experiments.

A PDP 11/44 computer was used for calibration, data acquisition, and experiment control. The system contained a 4-channel, 12-bit simultaneous sample-and-hold analog-to-digital converter which was used to digitize the anemometer signals at rates up to 20 kHz. Prior to the converter, signal conditioning on each channel consisted of a low-pass filter (used to prevent aliasing) and an amplifier with DC offset (to improve the digital resolution). For

automatic calibration and accurate setting of the experimental conditions, the wind tunnel blower speed was controlled by a digital-to-analog converter. A special DC motor-driven traverse with an optical position feedback sensor provided for accurate positioning of the X-wire in the Y direction (normal to the surface). The software used provided for automatic calibration, experiment control, data acquisition, on-line calculation of statistics, and off-line calculations with plotting and database management.

Power spectral density distributions were obtained by ensemble-averaging 40 spectral estimates, each resulting from fast Fourier transform (FFT) analysis of a record of 1024 values of velocity. The ensemble averages reported here have not been smoothed (no frequency filtering was used), and the spectral density $E(n)$ is normalized by the mean-square so that its integral over frequency is one.

REFERENCES

Blackwelder, R. F.: Hot-Wire and Hot-Film Anemometers. *Methods in Expt. Phys.: Fluid Dynamics*, vol. 18, pt. A, ed. R. J. Emrich, Academic Press, Inc., New York - London, 1981, pp. 259-314.

Bremhorst, K.: The Effect of Wire Length and Separation on X-Array Hot-Wire Anemometer Measurements. *IEEE Trans. on Inst. and Meas.*, vol. IM-21, no. 3, 1972, pp. 244-248.

Kuhn, W.; and Dressler, B.: Experimental Investigations on the Dynamic Behavior of Hot-Wire Probes. *J. Physics E.: Sci. Inst.*, vol. 18, 1985, pp. 614-622.

Ligrani, P. M.: *Subminiature Hot-Wire Sensor Construction.* Report No. NPS69-84-010, Naval Postgraduate School, Monterey, CA, Nov. 1984.

Ligrani, P. M.; and Bradshaw, P.: Subminiature Hot-Wire Sensors: Development and Use. *J. Physics E.: Sci. Inst.*, vol. 20, no. 3, Mar. 1987, pp. 323-332.

Ligrani, P. M.; and Bradshaw, P.: Spatial Resolution and Measurement of Turbulence in the Viscous Sublayer Using Subminiature Hot-Wire Sensors. *Expts. in Fluids*, vol. 5, 1987, pp. 407-417.

Lord, R. G.: The Dynamic Behavior of Hot-Wire Anemometers with Conduction End Losses. *J. Physics E.: Sci. Inst.*, vol. 14, no. 5, May 1981, pp. 573-578.

Miller, I. S.; Shah, D. A.; and Antonia, R. A.: A Constant-Temperature Hot-Wire Anemometer. *J. Physics E.: Sci. Inst.*, vol. 20, 1987, pp. 311-314.

Nakayama, A.; and Westphal, R. V.: *Effects of Sensor Length and Spacing on X-Wire Measurements in a Boundary Layer.* NASA TM-88352, Oct. 1986.

Perry, A. E.: *Hot Wire Anemometry.* Clarendon Press, Oxford University Press, England, 1982.

Perry, A. E.; Henbest, S.; and Chong, M. S.: A Theoretical and Experimental Study of Wall Turbulence. *J. Fluid Mech.*, vol. 165, 1986, pp. 163-199.

Roberts, J. B.: On the Correction of Hot-Wire Turbulence Measurements for Spatial Resolution Errors. *Aero. J.*, vol. 77, 1973, pp. 406-412.

Type 55M10 Instruction Manual, DISA 55M System with 55M10 CTA Standard Bridge, DISA Information Department, Franklin Lakes, N.J., 1982 (DISA is now DANTEC).

Westphal, R. V.; and Mehta, R. D.: *Crossed Hot-Wire Anemometry Data Acquisition and Reduction System.* NASA TM-85871, Jan. 1984.

Willmarth, W. W.; and Bogar, T. J.: Survey and New Measurements of Turbulent Structures Near the Wall. *Physics of Fluids*, vol. 20, no. 10, pt. II, 1977, p. S9-S21.

Willmarth, W. W.; and Sharma, L. K.: Study of Turbulent Structures with Hot-Wires Smaller than the Viscous Length. *J. Fluid Mech.*, vol. 142, no. , 1984, pp. 121-149.

Wood, D. H.; and Westphal, R. V.: *Measurements of the Free Stream Fluctuations Above a Turbulent Boundary Layer*. NASA TM 100036, Nov., 1987.

Wyngaard, J. C.: Measurement of Small-Scale Turbulence Structures with Hot-Wires. *J. Physics E.: Sci. Inst.*, vol. 1, series 2, 1968, pp. 1105-1108.

Wyngaard, J. C.: Spatial Resolution of the Vorticity Meter and other Hot-Wire Arrays. *J. Physics E.: Sci. Inst.*, vol. 2, series 2, 1969, pp. 983-987.

TABLE 1. - EQUIPMENT USED IN SUBMINIATURE PROBE FABRICATION.

	Item	Source
1.	Bausch & Lomb stereo zoom 7 coaxial illuminator microscope with variable transformer 115 0-115X	Scientific Instrument Co. Sunnyvale, CA
2.	3C INOX tweezers	A Dumont & Fils Switzerland
3.	razor knife and miniature broaching tool	–
4.	Electically conductive epoxy E-Solder No. 3021	ACME Division Allied Products Corp. New Haven, CT
5.	Wollaston wire .000025 in. diam. 90%platinum/10%rhodium	Sigmund Cohn Corp. 121 South Columbus Ave. Mount Vernon, N.Y.
6.	380128-7590 Schott Fiber Lite Source, 417053 Halogen Bulb 15-150W, 417058-9901 Double FO Light Guide 750 mm	Microscopes West, Inc. 475 N. Wolfe Road Sunnyvale, CA
7.	Double flask for etching and washing with pipette	Ames Code ETM Moffett Field, CA (custom equipment)
8.	Current controller	Raman Aeronautics Moffett Field, CA (custom equipment)
9.	Micropositioner Signatone model S-925LM (left-hand)	Signatone 3687 Enochs Street Santa Clara, CA

TABLE 2. - BOUNDARY LAYER PROPERTIES: $X = 295$ cm.

U_e, m/s	δ_{99}, cm	δ^*, mm	Re_θ	C_f	δ^*/θ
27.	3.8	5.82	8300.	0.00270	1.35

TABLE 3. - DIMENSIONS OF PROBES USED.

probe	d, μm	l, μm	s, μm	l/d	l^+	l/δ
NASA	5.0	800.	800.	160.	54.8	0.021
X2	0.63	210.	380.	336.	14.3	0.0055
S1	0.63	233.	-	373.	15.9	0.0061

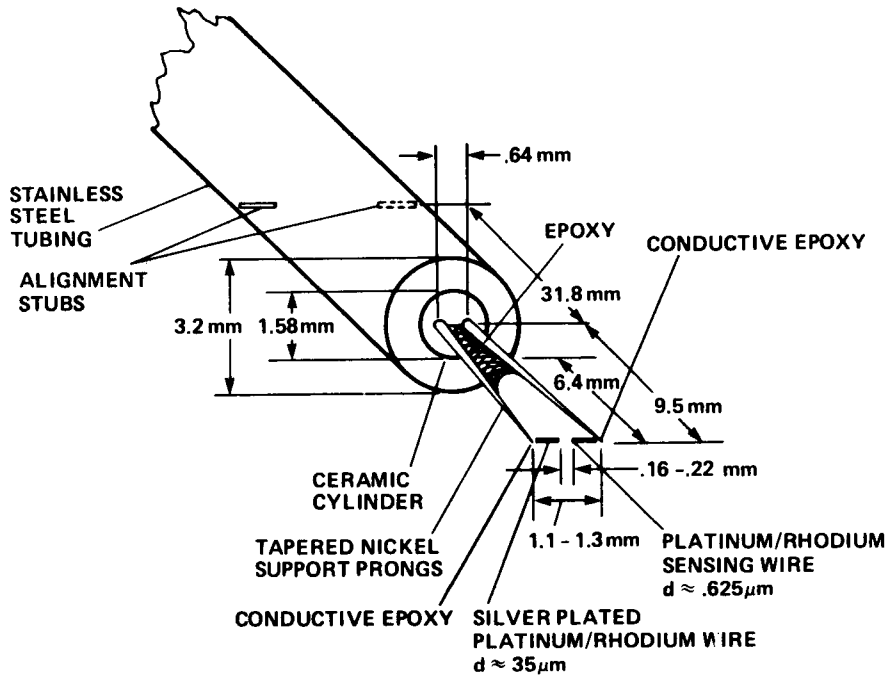

Figure 1. - Horizontal-wire sensor configuration.

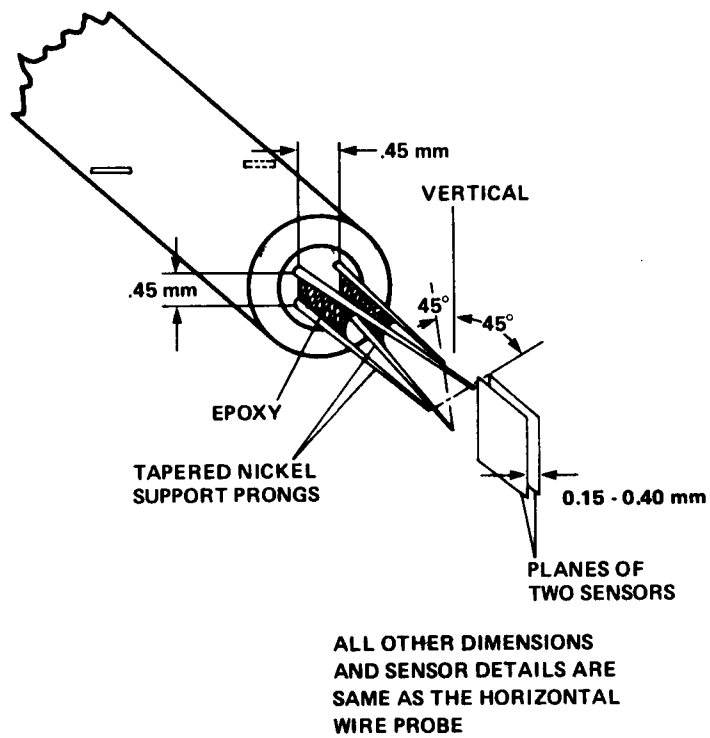

Figure 2. - Crossed-wire sensor configuration.

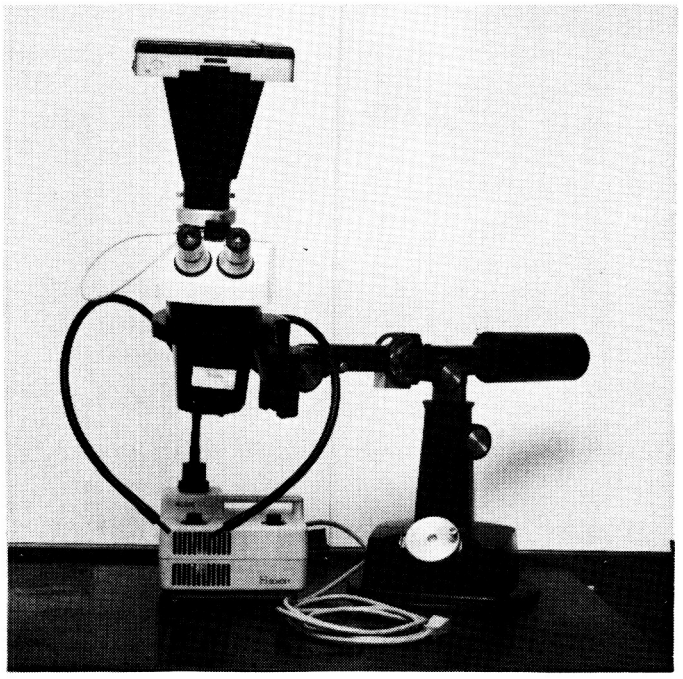

Figure 3. - Microscope and light source used for viewing and photographing the sensors during manufacture.

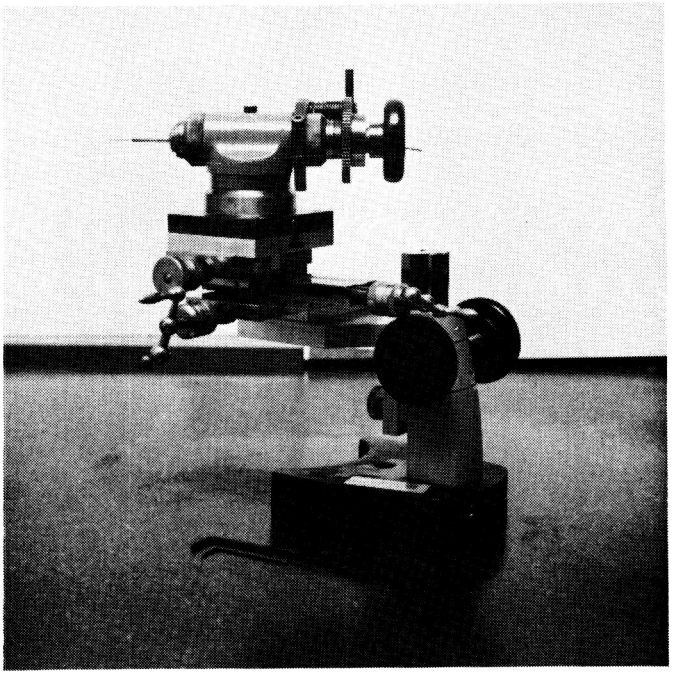

Figure 4. - Three-dimensional micromanipulator used to orient and position sensors during construction.

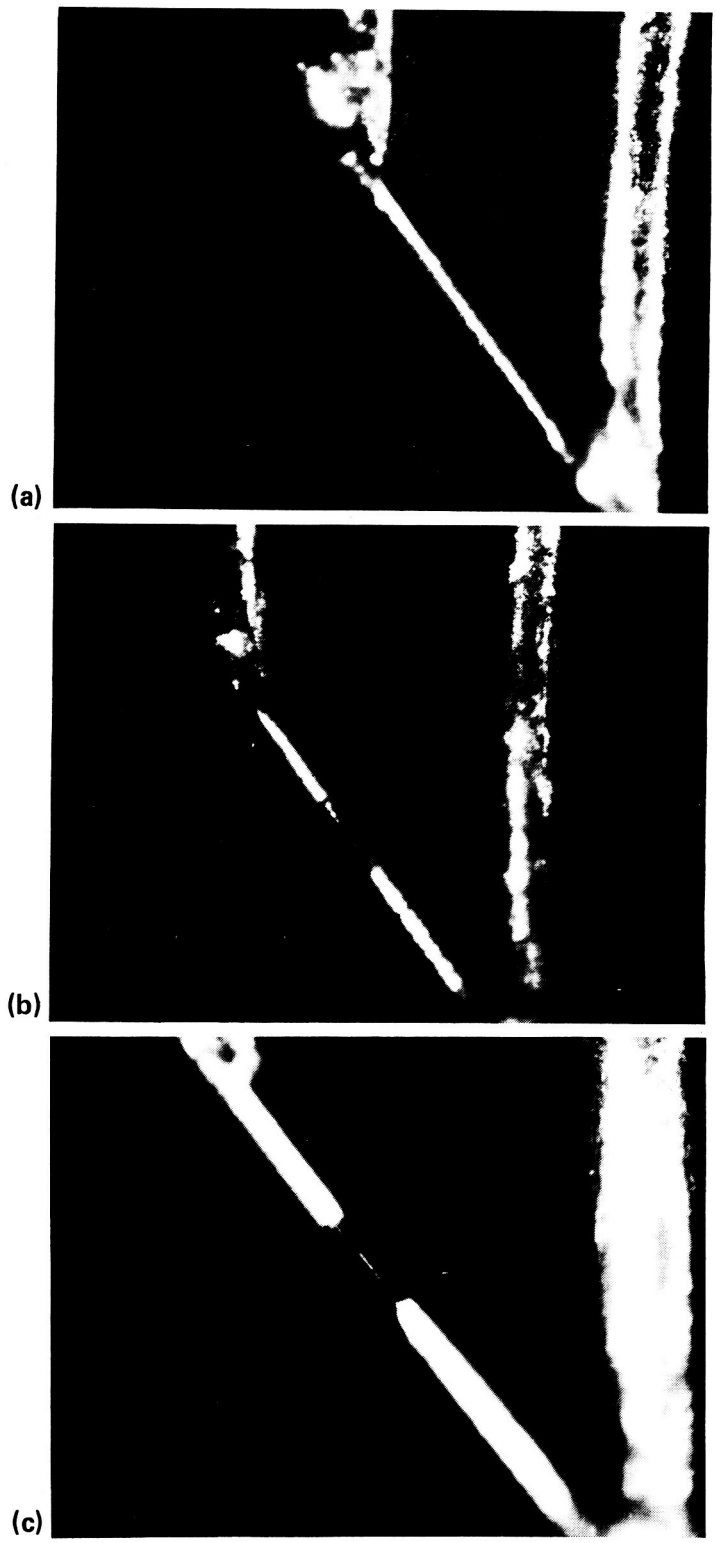

Figure 5. - Sensor appearance during construction, magnified 140 times. (a) Prongs with Wollaston wire epoxied into position. (b) Sensor as silver plating is removed during acid etching procedure. (c) Sensor after final washing at end of construction.

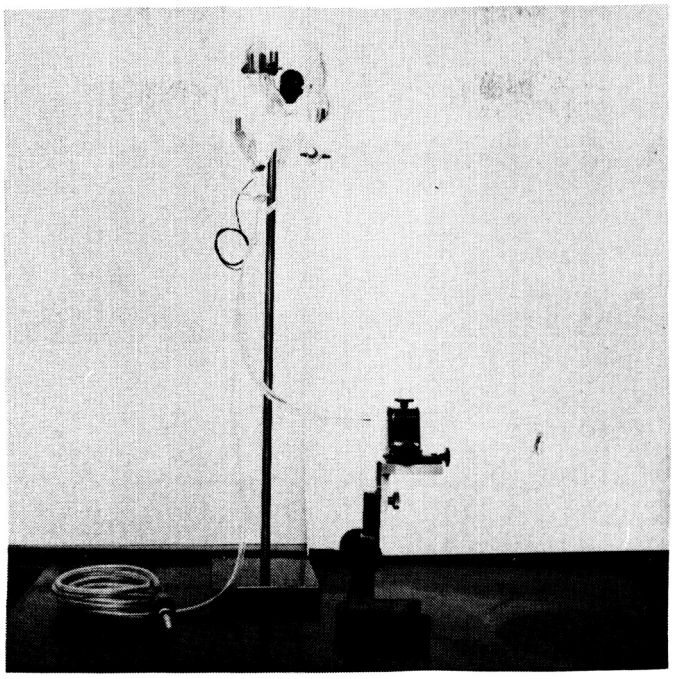

Figure 6. - Reservoir system with pipette used for etching and washing.

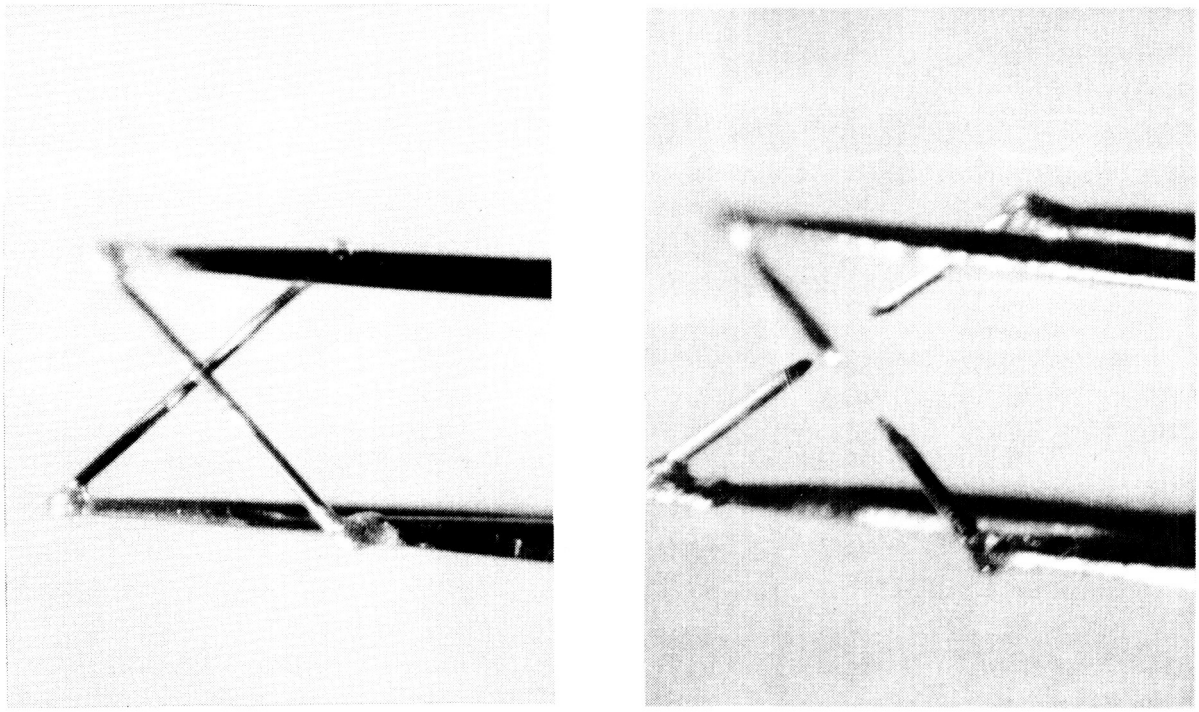

Figure 7. - Photograph of a subminiature crossed-wire probe, both before and after etching.

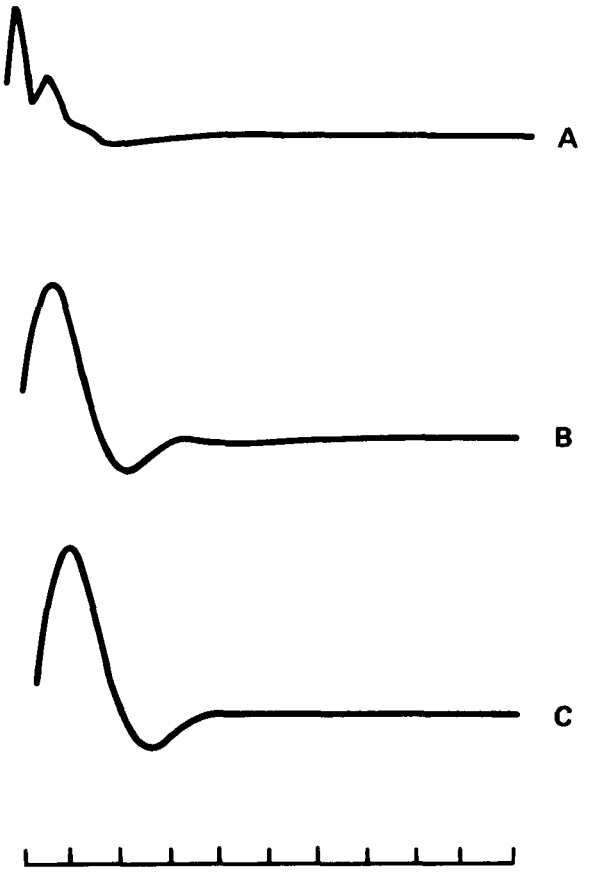

Figure 8. - Typical oscilloscope signal from subminiature sensor with a cold resistance of 130 ohms to a square-wave test. Curve A: r=1.2, 5 μs per division abscissa scale; curve B: r=1.5, 2 μs per division; curve C: r=1.65, 2 μs per division.

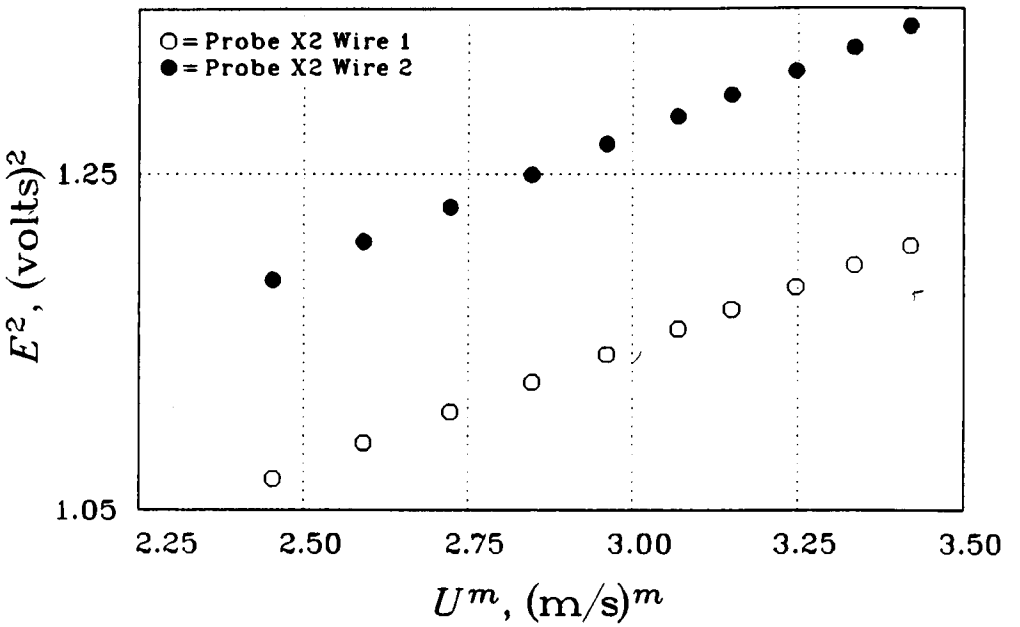

Figure 9. - Anemometer output vs. velocity calibration results for subminiature crossed-wire sensors. The calibration was performed over the range U_e = 10 to 30 m/s, and m = 2.7 has been used.

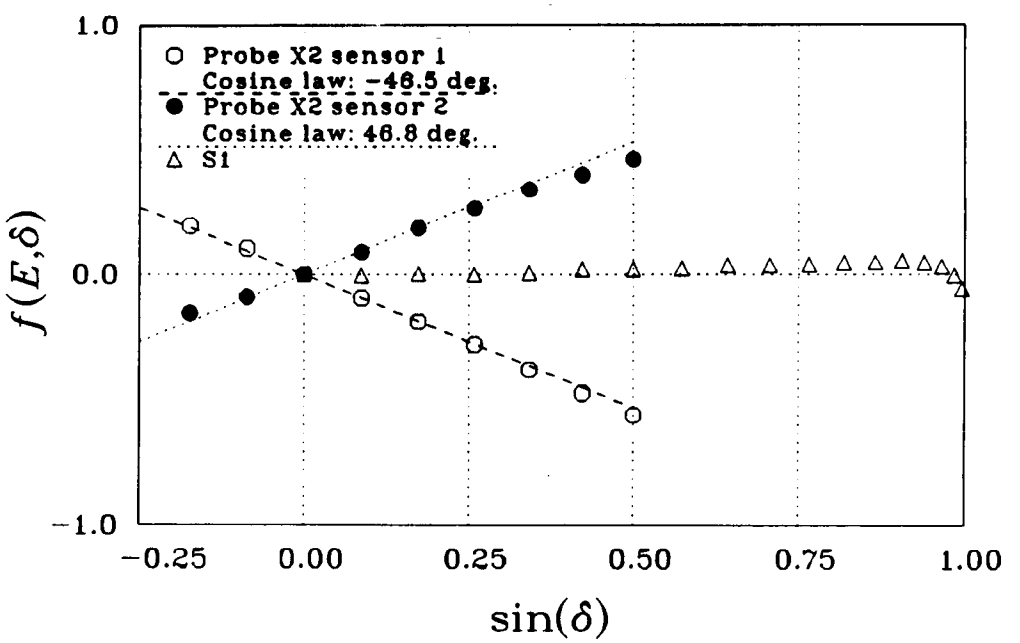

Figure 10. - Angular-response calibration characteristics of subminiature sensors at U_e = 20 m/s.

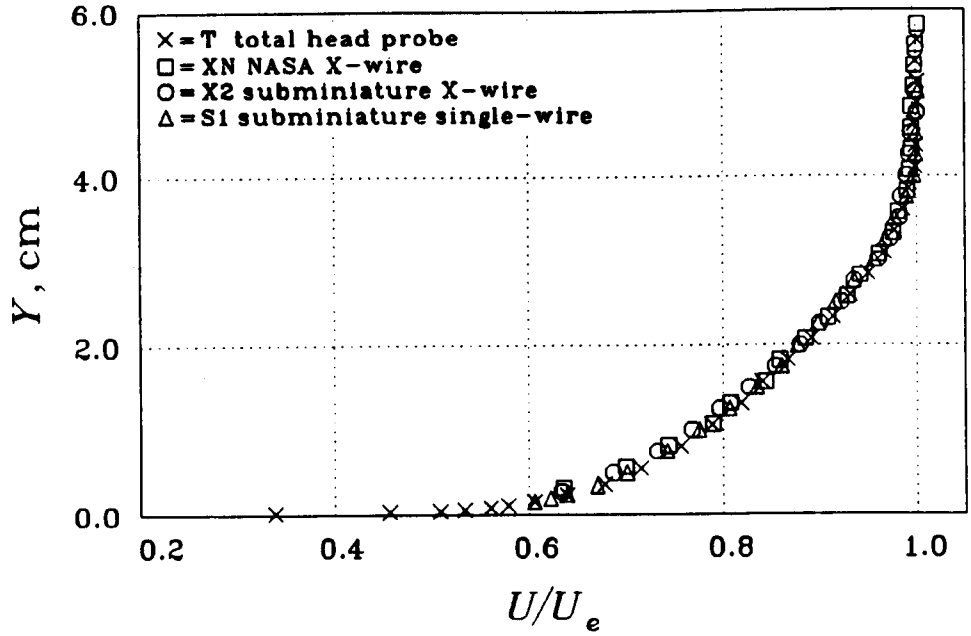

Figure 11. - Comparison of mean velocity profile measurements, $U_e = 27$ m/s.

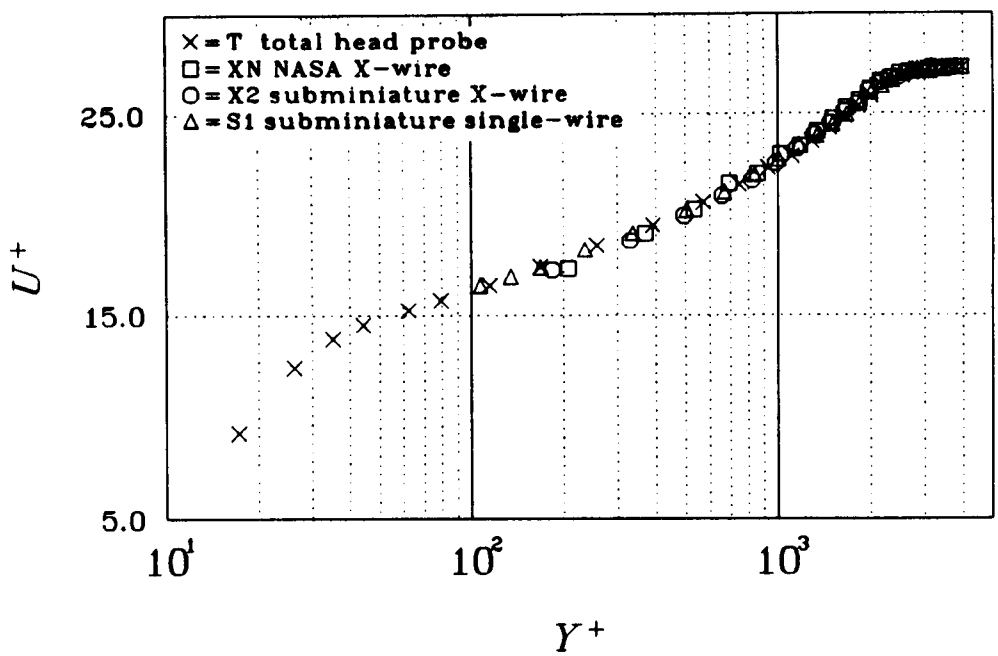

Figure 12. - Mean velocity profile measurements in inner coordinates, $U_e = 27$ m/s.

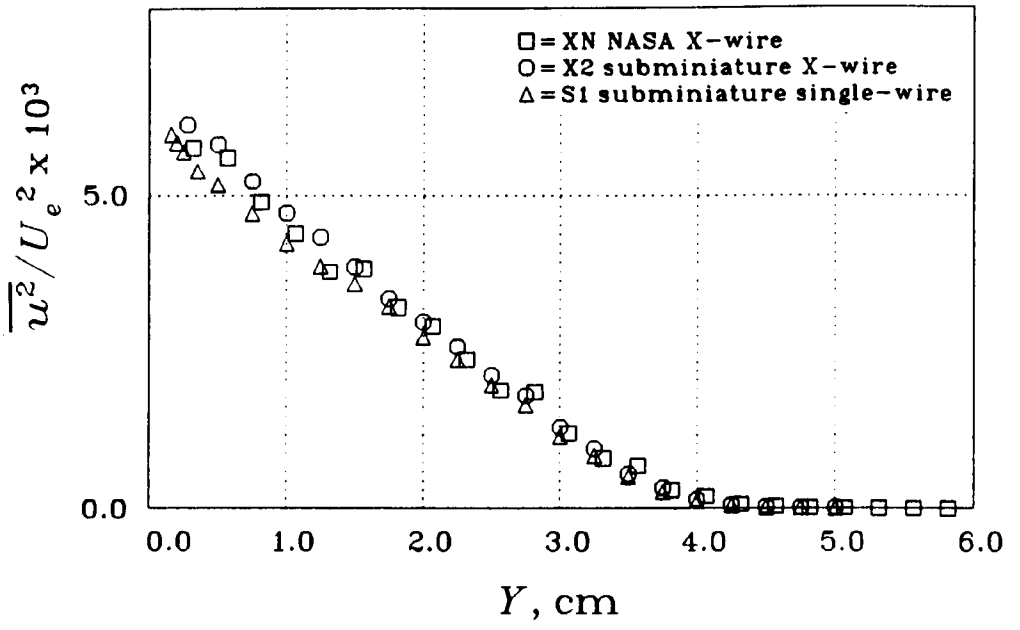

Figure 13. - Measurements of the normal Reynolds stress $\overline{u^2}$, $U_e = 27$ m/s.

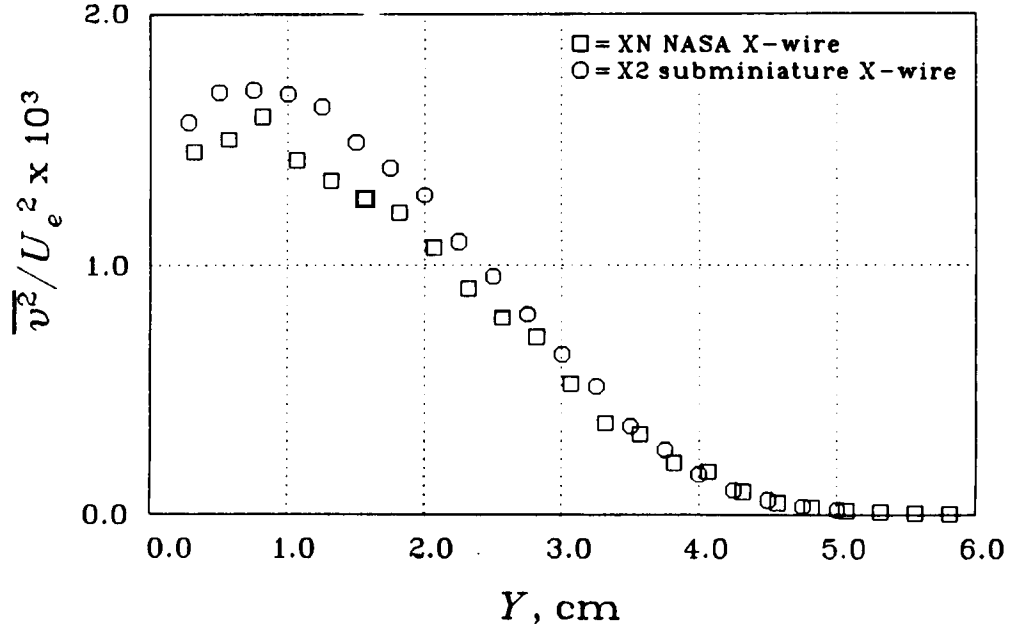

Figure 14. - Measurements of the normal Reynolds stress $\overline{v^2}$, $U_e = 27$ m/s.

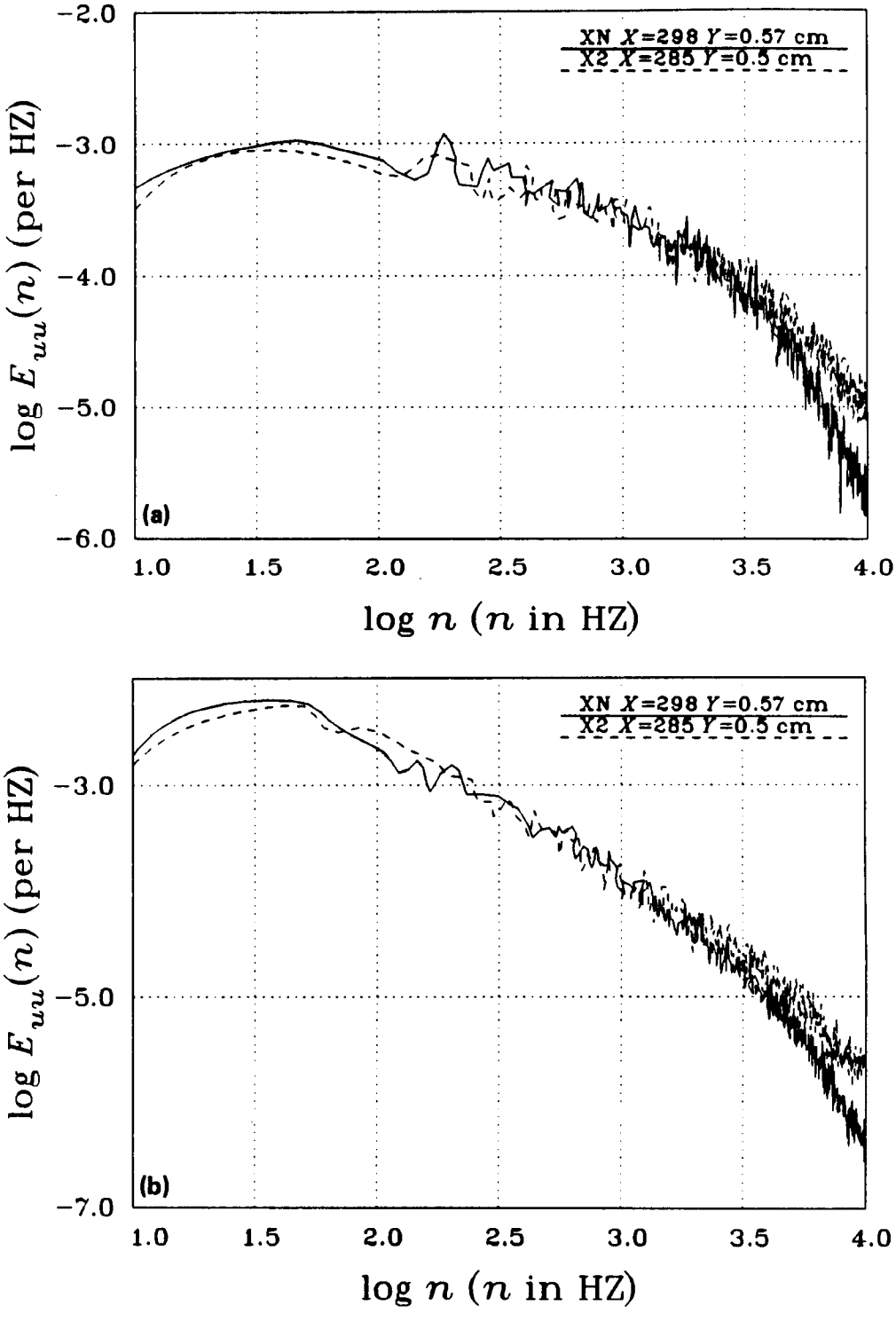

Figure 15. - Measurements of the spectral content of fluctuations in two normal stresses at $U_e = 27$ m/s and $Y^+ \sim 300$. (a) $E_{uu}(n)$, u spectra. (b) $E_{vv}(n)$, v spectra.

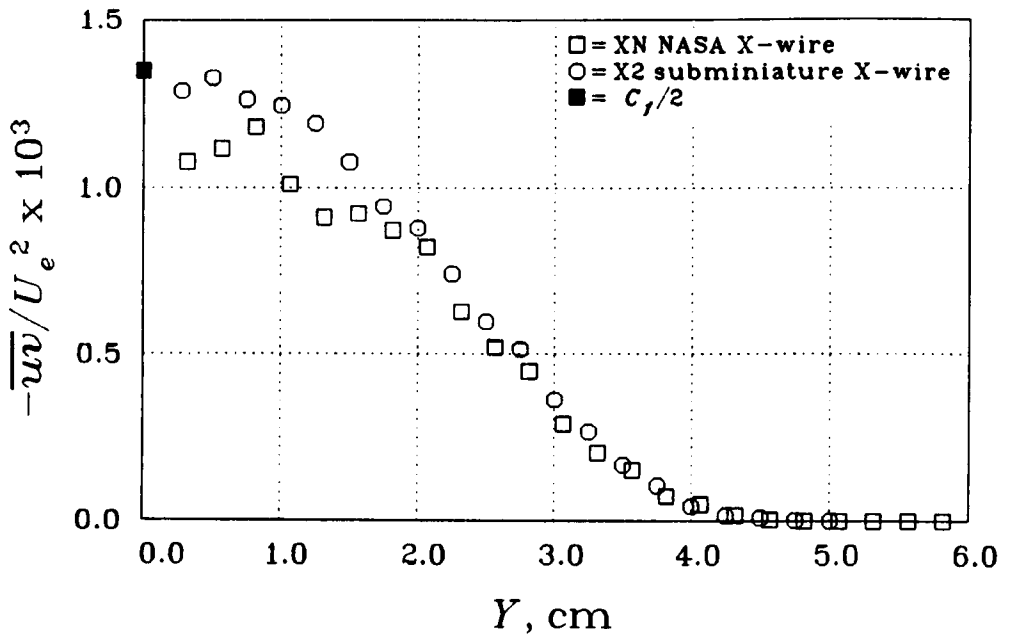

Figure 16. - Measurements of the Reynolds shear stress $\overline{uv}$, $U_e = 27$ m/s.

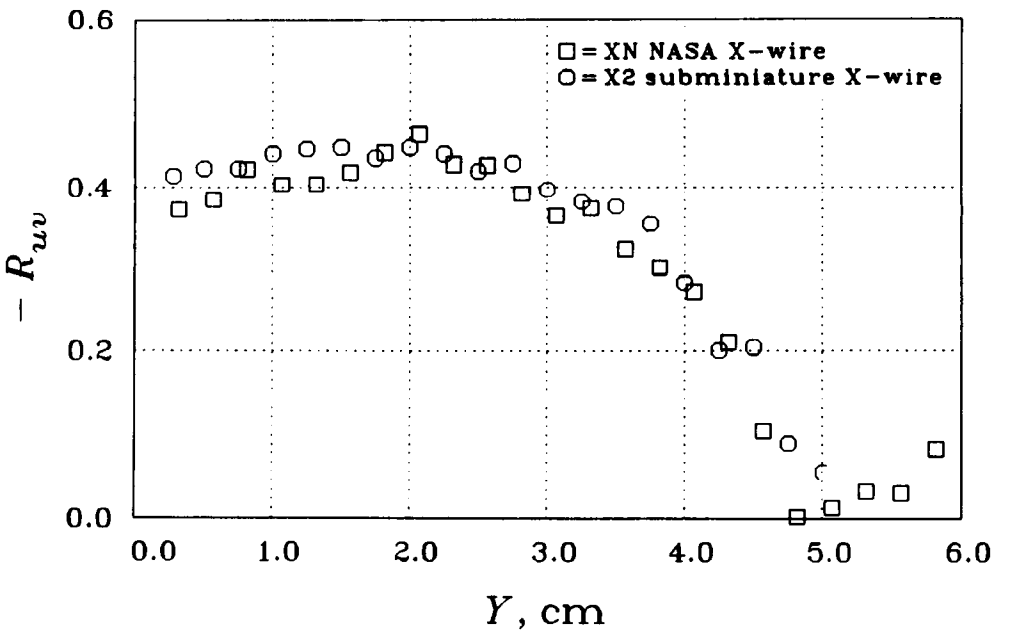

Figure 17. - Measurements of the correlation coefficient R_{uv}, $U_e = 27$ m/s.

NASA
National Aeronautics and Space Administration

Report Documentation Page

1. Report No.	2. Government Accession No.	3. Recipient's Catalog No.
NASA TM-100052		

4. Title and Subtitle	5. Report Date
Development of Subminiature Multi-Sensor Hot-Wire Probes	March 1988
	6. Performing Organization Code

7. Author(s)	8. Performing Organization Report No.
Russell V. Westphal, Phillip M. Ligrani (Naval Postgraduate School, Monterey, CA), and Fred R. Lemos	A-88045
	10. Work Unit No. 505-60-31
9. Performing Organization Name and Address	11. Contract or Grant No.
Ames Research Center Moffett Field, CA 94035	
	13. Type of Report and Period Covered
12. Sponsoring Agency Name and Address	Technical Memorandum
National Aeronautics and Space Administration Washington, DC 20546-0001	14. Sponsoring Agency Code

15. Supplementary Notes

Point of Contact: Russell V. Westphal, MS 260-1, Ames Research Center, Moffett Field, CA 94035
(415) 694-4140 or FTS 464-4140

16. Abstract

Limitations on the spatial resolution of multi-sensor hot-wire probes have precluded accurate measurements of Reynolds stresses very near ($Y^+ < 100$) solid surfaces in wind tunnels and in many practical aerodynamic flows. This report describes the fabrication, calibration, and qualification testing of very small, single horizontal and X-array hot-wire probes which are intended to be used near solid boundaries in turbulent flows where length scales are particularly small. Details of the sensor fabrication procedure are reported, along with information needed to successfully operate the probes. As compared with conventional probes, manufacture of the subminiature probes is more complex, requiring special equipment and careful handling. The subminiature probes tested were more fragile and shorter-lived than conventional probes; they obeyed the same calibration laws but with slightly larger experimental uncertainty. In spite of these disadvantages, measurements of mean statistical quantities and spectra demonstrate the ability of the subminiature sensors to provide measurements in the near-wall region of turbulent boundary layers that are more accurate than conventional-sized probes. Results obtained also point out the important and subtle effects of turbulence anisotropy on measurements from conventional probes.

17. Key Words (Suggested by Author(s))	18. Distribution Statement
Hot wire Turbulence Crossed wire Boundary layer Miniature	Unclassified – Unlimited Subject Category – 35

19. Security Classif. (of this report)	20. Security Classif. (of this page)	21. No. of pages	22. Price
Unclassified	Unclassified	32	A02